ACS APPLIED MATERIALS & INTERFACES

Research Article

www.acsami.org

Mimicry of Sputtered *i*-ZnO Thin Films Using Chemical Bath Deposition for Solution-Processed Solar Cells

Enrico Della Gaspera,* Joel van Embden, Anthony S. R. Chesman, Noel W. Duffy, and Jacek J. Jasieniak*

CSIRO Manufacturing Flagship, Bayview Avenue, Clayton, Victoria 3168, Australia

Supporting Information

ABSTRACT: Solution processing provides a versatile and inexpensive means to prepare functional materials with specifically designed properties. The current challenge is to mimic the structural, optical, and/or chemical properties of thin films fabricated by vacuum-based techniques using solution-based approaches. In this work we focus on ZnO to show that thin films grown using a simple, aqueous-based, chemical bath deposition (CBD) method can mimic the properties of sputtered coatings, provided that the kinetic and thermodynamic reaction parameters are carefully tuned. The role of these parameters toward growing highly oriented and dense ZnO thin films is fully elucidated through detailed microscopic and spectroscopic investigations. The prepared samples exhibit bulk-like optical properties, are intrinsic in their electronic characteristics, and possess negligible organic contaminants, especially when compared to ZnO layers deposited by sol–gel or from nanocrystal inks. The efficacy of our CBD-grown ZnO thin films is demonstrated through the effective replacement of sputtered ZnO buffer layers within high efficiency solution processed $Cu_2ZnSnS_{4x}Se_{4(1-x)}$ solar cells.

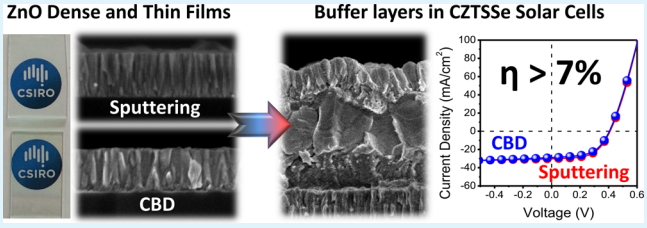

KEYWORDS: *CBD, solution processing, CZTS, zinc oxide, optoelectronics*

INTRODUCTION

Solution processing offers unprecedented control of the structural, chemical, and optical properties of materials, particularly at the nanoscale.[1−7] This enables the possibility to develop novel, low-cost, and high-performance optoelectronic devices, as well as to improve existing technologies that utilize alternative deposition methods.[8] Despite these benefits there is a strong belief that vacuum processes, such as sputtering, chemical/physical vapor deposition, and thermal evaporation are superior for the fabrication of most optoelectronic devices.[9−11] In this work we focus on the chemical bath deposition (CBD) of zinc oxide (ZnO), and we challenge this assumption by demonstrating that, through careful manipulation of the reaction conditions, the deposition method outlined herein can readily mimic those of ZnO prepared by standard vacuum-based methods.

ZnO is one of the most studied materials for optoelectronics due to its transparency, excellent electrical properties, high exciton binding energy, and structural anisotropy.[12−14] While ZnO is most commonly deposited using vacuum-based processes, it has also been processed using solution-based techniques, mainly through sol–gel methods or nanoparticle (NP) "inks", and subsequently employed within light-emitting diodes,[15] transistors,[16,17] solar cells,[18,19] and sensors.[20,21] The simplicity of these wet chemical deposition techniques is also met with major caveats, particularly at low processing temperatures, including high porosity, poor electronic properties, and low crystallinity of the deposited films.[22,23] For these reasons, further improvements are envisaged if the ZnO layers could be prepared with the structural and electronic properties akin to vacuum processes at low temperatures.

To address these issues, we have adapted a CBD synthesis that was originally developed to prepare arrays of ZnO nanowires (NWs). The seeded growth of ZnO NWs relies on the condensation of zinc hydroxo-species formed in an aqueous solution in the presence of an organic amine.[24−26] These arrays have been widely applied in catalysis, photodetectors, and organic, inorganic, and dye-sensitized solar cells.[27−31] The successful implementation of ZnO arrays within such applications hinges upon the ability to control the structure of these arrays at the nanoscale. It is widely known that the CBD method enables for the synthesis of a wide range of ZnO architectures.[25,32,33] However, of all the currently available ZnO architectures, none have been made that possess a well-controlled morphology at very low thicknesses. In this work, by using optimized seed layers and CBD conditions, we demonstrate the deposition of dense, thin (<300 nm), and oriented films, analogous to those obtained through sputtering.

Such ZnO films are ideal candidates for replacing equivalent sputtered layers in many optoelectronic applications. Within inorganic solar cells, for instance, particularly those fabricated in a "substrate" configuration (see Figure 1a), such layers provide electronic buffering to improve both the reliability and the efficiency of the device.[34−38] The ZnO in this case prevents

Received: September 26, 2014
Accepted: December 4, 2014
Published: December 15, 2014

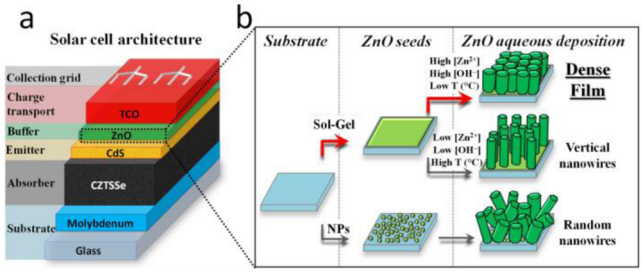

Figure 1. Schematic representation of (a) the conventional substrate architecture for CZTSSe solar cells; (b) the ZnO structures that can be obtained through aqueous CBD. The red arrows highlight the strategy used in this work to obtain thin and dense ZnO films.

direct contact of the transparent conductive oxide (TCO) with the n-type emitter (commonly CdS), causing an enhanced shunt resistance and, consequently, maximizing the open-circuit voltage. If the buffer layer is too thick, series resistance limitations reduce solar cell performance.[35−38] Also, if porous or inhomogeneous films are used, they do not provide a sufficient barrier to prevent shunting paths between TCO and the n-type layer.[37,38] Therefore, only intrinsic, homogeneous, and dense thin films result in enhanced performance and reliability of solar cells.

To date, no alternative to sputtering such intrinsic ZnO (*i*-ZnO) buffer layers has been demonstrated due to the difficulty in fulfilling each of the above requirements. The ZnO layers grown here overcome these challenges by mimicking the structure and properties of sputtered films. In addition, they also compliment the growing research effort toward developing all-solution-processed inorganic solar cells.[39−43] The efficacy of the method developed here is demonstrated by incorporating these ZnO layers into $Cu_2ZnSnS_{4x}Se_{4(1-x)}$ (CZTSSe)-based solar cells processed from solution. Importantly, identical device characteristics are achieved for sputtered and CBD grown ZnO, with devices reaching power conversion efficiencies (PCE) of over 7%.

EXPERIMENTAL SECTION

All chemicals are reagent grade, and they were used without further purification.

Sol−Gel Seed Layer. To prepare the sol−gel solution for ZnO seeds, zinc acetate dihydrate (Analar, 99.5%) was dissolved in methoxyethanol (Merck, 99.5%) to a concentration of 0.1 M in the presence of ethanolamine (Sigma-Aldrich, 99%) in a 1:1 molar ratio with zinc. Seed layers were deposited by spin coating at 2000 rpm for 30 s, and then the films were annealed at 180 °C in air for 5 min on a hot plate. This procedure was repeated again to ensure homogeneous coverage of seeds on the substrates, with the final samples annealed at 180 °C for 10 min.

Chemical Bath Deposition of ZnO Films. An aqueous solution (90 mL, 83 mM) of zinc nitrate hexahydrate (Sigma-Aldrich, 99%) was preheated in a water bath at 70 °C. The pH of the zinc nitrate solution was adjusted to ∼7 using a 25% ammonium hydroxide solution in water (Chem Supply), and then the substrates were dipped with the seeded surface slightly facing downward and left for 5 min to thermally equilibrate the temperature. Separately, hexamethylenetetramine (HMTA, Sigma-Aldrich, 99%) was dissolved in 10 mL of water at room temperature to give a 0.75 M solution, which was then added to the zinc nitrate solution, and the samples were kept in the bath for 30−60 min to obtain a thickness in the 100−150 nm range. The process to achieve these optimized conditions involved variation of concentration of species, temperature, pH, and duration of the chemical bath deposition, as discussed in the manuscript and summarized in Supporting Information, Table S1. After the deposition, samples were carefully rinsed with water, ultrasonicated for 2 min in ethanol to remove surface precipitates, and eventually dried with a nitrogen stream.

ZnO films were deposited on properly seeded silicon or glass substrates to perform the desired characterizations. Parallel depositions using CdS-coated substrates where the CdS layer is deposited via CBD using a published procedure were also carried out.[44] For impedance measurements, ZnO films were deposited on patterned ITO/glass substrates and subsequently covered with a Spiro-OMeTAD-based layer prepared using a published procedure.[45] The diodes were completed by evaporating silver top contacts (200 nm thick) through a shadow mask defining an active device area of 0.1 cm^2.

Other solution-processed ZnO films were prepared for comparison: in detail, ZnO colloids were synthesized using the method published by Wood et al.,[46] and the films were deposited by spin-coating a colloidal solution of the NPs in ethanol. Sol−gel films were deposited using the same procedure adopted for the seed layers preparation, but using a 0.7 M solution. These films were eventually annealed at 180 or 400 °C.

CZTSSe Solar Cells. The solar cells were prepared using the standard device structure in a substrate configuration: glass/Mo/CZTSSe/CdS/ZnO/ITO/Al. The absorbing layer was deposited by spin coating a colloidal solution of Cu_2ZnSnS_4 NPs on molybdenum-coated glass substrates. The nanocrystalline films were subsequently annealed in selenium-rich atmosphere under argon. The CdS layer was deposited by chemical bath deposition, ZnO was deposited either by direct current (DC) sputtering or chemical bath deposition as described above, ITO was deposited by radio frequency (RF) sputtering, and eventually Al collection grid was thermally evaporated. The final devices were defined by mechanical scribing to provide total (active) areas of 0.5 cm^2 (0.37 cm^2) as measured with optical microscopy. Details on the CZTSSe deposition procedure and on the solar cells fabrication are reported elsewhere.[44]

Characterization. The morphology of the deposited films was investigated using an FEI Helios Nanolab 600 scanning electron microscope (SEM). X-ray diffraction (XRD) patterns of the deposited films were collected using a Bruker D8 diffractometer equipped with a Cu Kα radiation source and operated at 40 mV and 40 mA. The average surface roughness of the samples was evaluated using a Veeco Dektak 6 M profilometer. Optical absorption spectra of films deposited on glass substrates were measured using a Varian-Cary 5E spectrophotometer. Ellipsometry quantities Ψ and Δ were measured using a J.A. Woollam M-2000 spectroscopic ellipsometer, and the refractive index was evaluated from Ψ and Δ data using the CompleteEASE data analysis software. Fourier-transform infrared spectroscopy (FTIR) measurements on samples deposited on Si substrates were performed using a Thermo Scientific Nicolet 6700 instrument. Ultraviolet photoelectron spectroscopy (UPS) was carried out on a Kratos Axis-HSi instrument using He I 21.1 eV radiation. Samples for these experiments were deposited on silicon substrates. The Fermi edge of a clean Au film was used as the 0 eV reference, and all samples were measured under a −9 V bias to separate the sample and analyzer low-energy cutoff. Impedance spectroscopy measurements were conducted using a Solartron SI 1255 frequency response analyzer combined with a Solartron SI 1286 electrochemical interface. The measurements were carried out using an applied voltage of −0.1 V with an alternating current (AC) amplitude of 10 mV over a frequency range of 10^2−10^6 Hz. The data were collected and analyzed using Zview and Zplot software, with fitting performed using an equivalent RC circuit that featured a constant phase capacitive element (CPE). The final values were determined from an average of three devices. CZTSSe solar cells fabricated as described earlier were tested with an Oriel solar simulator fitted with a 1000 W Xe lamp filtered to give an output of 100 mW cm^{-2} at AM 1.5. Current−Voltage (J−V) curves were obtained using a Keithley 2400 sourcemeter controlled by Labview Software.

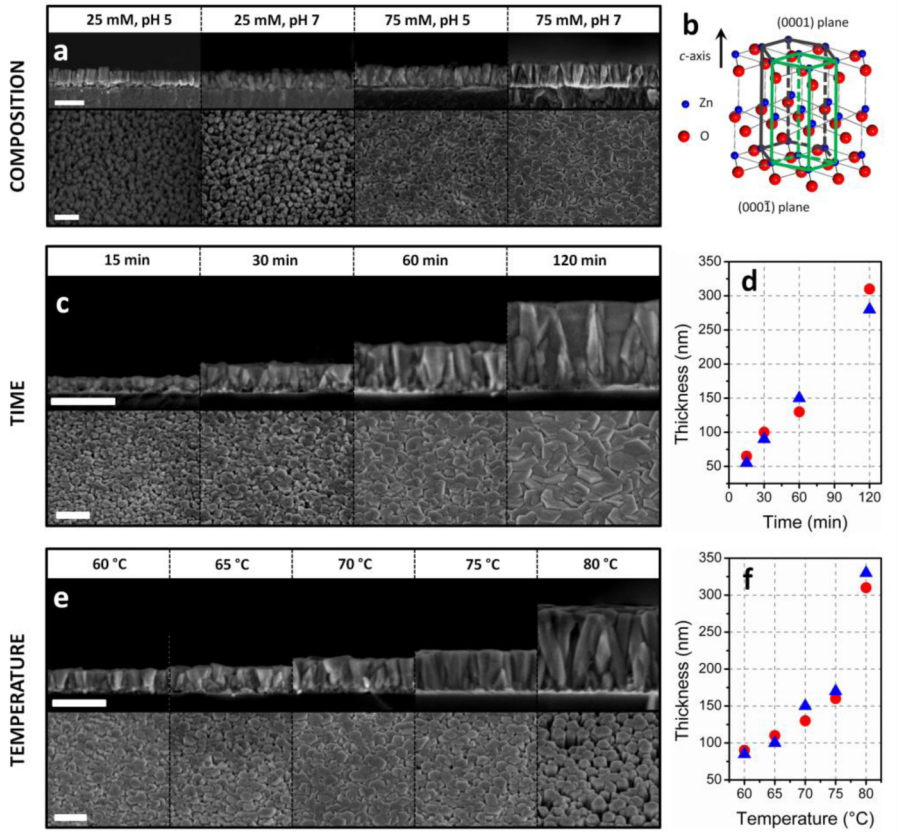

Figure 2. (a) SEM images in cross section (upper images) and top view (lower images) of ZnO films grown by CBD at 70 °C for 1 h with different bath compositions. (b) Schematic representation of the wurtzite ZnO crystalline cell. (c) SEM images in cross section and top view of ZnO films grown by CBD at 70 °C with different reaction times. (d) Evolution of ZnO thickness with time during two different depositions as measured from SEM images. (e) SEM images in cross section and top view of ZnO films grown by CBD for 1 h at different bath temperatures. (f) Evolution of ZnO thickness with temperature as measured from SEM images. All scale bars are 200 nm, and the top scale bar is common to all cross sections, while the bottom scale bar is common to all top views.

RESULTS AND DISCUSSION

The general synthetic approach used in this study for fabricating structurally controlled ZnO layers via CBD is shown in Figure 1b. The CBD process was carried out on seeded substrates using an aqueous solution of zinc nitrate in the presence of an organic amine (HMTA) at a controlled pH. We first turn our attention to the ZnO seed layer. The quality of the seed layer is critical as it provides the necessary heterogeneous growth sites to define the morphology of the final film. Two types of ZnO seeds were assessed here, namely those prepared via a colloidal NP method and a sol–gel approach. In the case of the NP seeds, their random orientation culminated in the growth of randomly oriented nanowires (Figure S1). This prevented the transformation of such layers into dense thin films. In contrast, sol–gel seeds provided (crystallographically) highly oriented samples (see Figure S2), which are ideal for directing the vertical growth of ZnO.[47]

The sol–gel seed layers were deposited with a minimal thickness (10–15 nm as measured with ellipsometry) that ensured a homogeneous and uniform coating of the substrate. The seed layer was then annealed at 180 °C in air to reach the onset of crystallization. At this temperature, seed crystallites of ~5 nm with a density of $\sim 6 \times 10^{11}$ cm^{-2} were observed, which grew into ZnO pillars with a density of $\sim 8 \times 10^{10}$ cm^{-2} after CBD. This high density of vertically oriented ZnO rods is ideal for obtaining continuous and dense films. At higher temperatures, larger seeds (up to 40 nm) with lower areal density (~7 $\times 10^{10}$ cm^{-2}) were obtained, which caused the nucleation of a lower density of ZnO pillars at $\sim 3 \times 10^{10}$ cm^{-2}. Although these low-density seed layers provide an ideal template for fabricating sparse arrays of isolated nanowires (Figure S1), they do not promote the formation of dense thin films, which is the goal of this work. We note that seeds annealed at temperatures below 180 °C were found to be unstable when dipped into the chemical bath, and that ZnO growth was not achieved on unseeded samples, regardless of the substrate.

Figure 2a shows the SEM micrographs of ZnO layers deposited from chemical baths with different compositions. It is well-established that the final ZnO microstructure is drastically affected by the composition of the chemical bath.[48,49] To obtain thin, vertically aligned, and dense ZnO coatings, the relative growth along the *c*-axis of the hexagonal cell must be reduced with respect to lateral directions. Fundamentally, one-dimensional ZnO structures grow preferentially along the *c*-axis, because the polar Zn-terminated (0001) and O-terminated (000$\bar{1}$) planes possess the highest energy among the low-index surfaces (see Figure 2b).[47,50] The natural polarity of these planes may be taken advantage of to limit growth along the vertical (thermodynamically preferred) direction. It has been shown that the (000$\bar{1}$) surface is highly unstable and reacts readily when in contact with water to form hydroxyl groups. Meanwhile, the (0001) surface has a strong tendency to adsorb polar or charged species, such as alcohols, carboxylic acids, or OH^- groups.[50−52] Such adsorbates can therefore limit the

dx.doi.org/10.1021/am506611j | ACS Appl. Mater. Interfaces 2014, 6, 22519−22526

growth along the *c*-axis compared to lateral directions. While this phenomenon is undesirable when growing arrays of NWs with high aspect ratios, it has been exploited here to achieve dense and thin coatings.

During the deposition of ZnO from a dilute solution of reagents commonly adopted for NW synthesis ([Zn] = 25 mM; [HMTA] = 25 mM), we obtained arrays of thin nanorods, which eventually evolved into long wires if the temperature and/or the reaction time were increased.[31] Upon increasing the concentration of the reagents ([Zn] = 75 mM; [HMTA] = 75 mM), we obtained denser and thicker coatings composed of larger rods. These differences are consistent with (i) the faster nucleation and growth kinetics at higher precursor concentrations and (ii) the enhanced lateral growth dynamics resulting from the larger [OH^-] at the increased [HMTA].[25,53,54] The relative axial growth rates can also be explicitly controlled by modifying the pH using aqueous ammonia.[55] It was found that ZnO structures grown at neutral pH showed increased lateral growth with respect to samples synthesized under acidic conditions (see also Figure S3). By combining high reagent concentrations with small and evenly distributed sol–gel seeds, dense ZnO films composed of highly oriented rods could be formed. Notably, the ZnO coatings formed from a solution buffered with ammonia to a pH ≈ 7 were of a higher quality and more reproducible compared to films grown at lower pH values. This may be attributed to more controlled growth and a higher stability of the underlying ZnO seed layer at neutral pH.

In addition to these conditions, time and temperature also play a fundamental role in defining the final morphology of the deposited films. Figure 2c shows cross-sectional and topographic SEM images of the ZnO film grown using our optimized reaction conditions and a bath temperature of 70 °C. During the initial stages of the CBD (<15 min), ZnO deposition results in the formation of short rods and in the incomplete coating of the substrate. As the ZnO rods continue to grow, after ∼30 min, the ZnO microstructure densifies to form a thin (∼100 nm) uniform coating. Longer reaction times resulted in thicker films with little change to the overall film morphology, despite a slight increase in surface roughness, due to further crystal growth (see Table S2). During the 2 h reaction window investigated here, these films were found to grow linearly with time along the *c*-axis at a growth rate of ∼2.2 nm/min (Figure 2d). Interestingly, this growth rate is approximately the same as that typically utilized for sputtering ZnO layers (∼2–3 nm/min). Notably, the average lateral size of the ZnO rods also progressively grew throughout the reaction. From statistical characterization we calculate a lateral growth rate of ∼0.8 nm/min (see Figure S4).

The effect of temperature has an equally important role on the final ZnO structure. This is demonstrated in Figure 2e,f for systems grown for 60 min. It can be seen that in the low-temperature regime (<80 °C), dense ZnO thin films form with a thickness that progressively increases with temperature. However, at 80 °C (and above) the growth conditions become modified, enhancing the relative growth along the *c*-axis. This results in a significant increase to the overall film growth rate (∼5.3 nm/min) at the cost of growing more isolated nanowire arrays. This increase is consistent with growth rates reported in the literature for ZnO NWs deposited at high temperature, for example ∼16 nm/min at 95 °C.[24] Collectively, these results demonstrate that through the judicial use of high Zn and HMTA concentrations, neutral pH, temperatures below 80 °C, and the use of sol–gel seed layers, CBD can be used to deliver dense and thin ZnO films. A summary of the optimized conditions is presented in Table S1.

To compare the microstructural properties of the ZnO thin films developed here to those of sputtered layers, we fabricated thin films of a nominal thickness of 150 nm via each method. In Figure 3a,b we show SEM images of these samples, respectively.

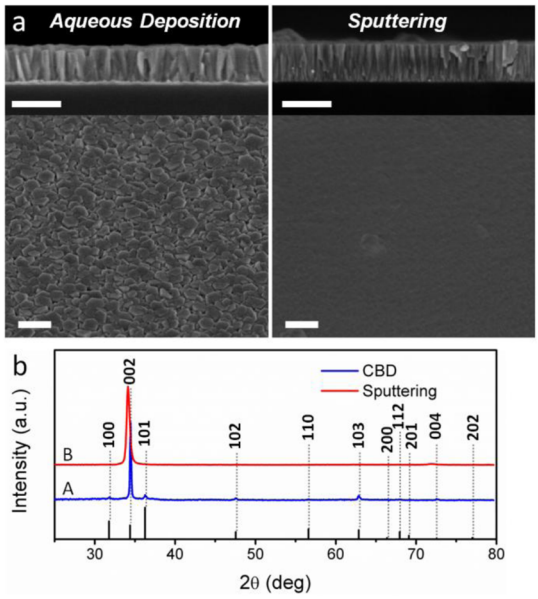

Figure 3. (a) SEM images of ZnO films deposited by CBD (left) and with sputtering (right) in cross section (upper images) and top view (lower images). All scale bars are 200 nm. (b) XRD patterns of ZnO films from CBD (scan A) and from sputtering (scan B). The reference pattern for wurtzite ZnO (ICDD No. 36–1451) is reported at the bottom.

Both films are composed of anisotropic ZnO nanorods, which are both highly oriented and densely packed. The width of the rods prepared by CBD is slightly larger compared to the sputtered sample. In addition, the surface roughness of the films prepared with these two contrasting techniques is similar (see Table S2). Structurally, both samples exhibit strong alignment along the *c*-axis of wurtzite ZnO (ICDD No. 36–1451), as is evident from the prominent (002) diffraction peak observed in the XRD patterns (Figure 3c). This peak is slightly broader in the sputtered sample, indicating smaller crystals, consistent with SEM observations. We note that even though the ZnO films deposited from chemical bath are highly oriented, they do show very weak, secondary diffraction peaks. Despite this, determination of the texture coefficient reveals that CBD produces films with an alignment factor as high as 90% (see Figure S2 and Table S3)—an unprecedented value for alternative solution-processed ZnO layers.[56]

Ultimately, the structural, optical, chemical, and electronic properties must be equivalent to claim mimicry of sputtered ZnO by our CBD method. To this extent, we employed various spectroscopic techniques to better appreciate these properties (see Figure 4). From an optical perspective, the as-deposited ZnO films are highly transparent in the visible range and show a strong UV absorption onset at ∼380 nm, indicative of bulk ZnO (Figure 4a). Moreover, when the films were deposited on seeded CdS films, as dictated by the substrate architecture of the solar cells outlined earlier, the optical properties of the ZnO films remain unchanged (Figure 4a). Specifically, these optical

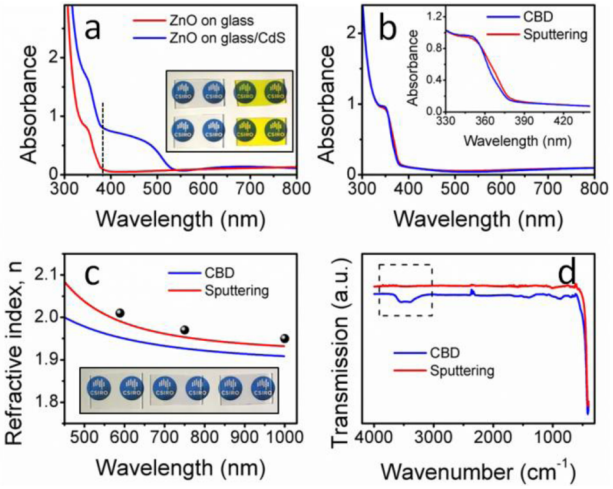

Figure 4. (a) Optical absorption spectra of ZnO films from CBD grown on glass and glass-CdS substrate. The dashed line highlights the UV absorption onset of ZnO. (inset) A picture of the ZnO sample on glass (upper left) and on glass/CdS (upper right); the glass and glass/CdS substrates are also reported (lower left and right). (b) Optical absorption spectra of ZnO films from CBD and from sputtering of similar thickness deposited on glass substrates. (inset) An enlarged view of the UV absorption onset. (c) Refractive index curves for ZnO films from CBD and from sputtering. The values for bulk ZnO are reported as black dots.[57] (inset) A picture of (left to right): glass substrate, ZnO from CBD and sputtered ZnO. (d) FTIR spectra of ZnO films from CBD and from sputtering; the spectra are offset vertically for clarity. The box highlights the range of −OH vibrations.

properties are identical to those of sputtered ZnO (Figure 4b). The similarity in the optical absorption profile resulting from these two contrasting deposition techniques is supported by ellipsometric measurements (Figure 4c), which demonstrate comparable refractive index values close to 2 in the visible range (bulk ZnO has a refractive index value of 2.01 at 589 nm).[57] The ∼2% lower values of the CBD grown films are ascribed to residual porosity present in the solution-processed films, especially closer to the ZnO seed layer. Using the Bruggeman effective medium model, the pore volume fraction has been estimated to be less than 2% in the sputtered film and ∼5% in the film deposited from chemical bath.[58] Importantly, the refractive index of the ZnO grown by CBD is much larger than that of coatings prepared by more conventional solution-based methods such as NP and sol−gel (see Figure S5 and Table S4), which have higher porosity (35−40%), lower crystallinity, and smaller grain sizes (see also Figure S2).

FTIR spectroscopy, which probes the chemical signatures of the materials, shows that sputtered ZnO films exhibit only the 440 cm^{-1} Zn−O stretching vibration,[59] while those prepared via CBD also show the residual −OH vibrations in the 3000−3500 cm^{-1} range (Figure 4d). The latter observation is consistent with the aqueous CBD deposition process, which proceeds through Zn−OH intermediates, and the lack of any post deposition thermal treatments. Importantly, the samples exhibit no organic impurities, which are typically observed in ZnO films made using sol−gel or NP-based approaches (Figure S6).

In addition to the optical characterization, we used ultraviolet photoelectron spectroscopy (UPS) to evaluate the electronic structure of the various ZnO films assessed here (see Figure S7 and Table S5). The films deposited by sputtering and chemical bath exhibit almost identical band structure, with the conduction band, valence band, and Fermi energy values versus vacuum being −3.8, −7.2, and −3.9 eV, respectively. For comparison, the Fermi energy levels of ZnO layers deposited from sol−gel and NP solutions show a shift toward the conduction band edge, indicating the formation of highly n-type doped ZnO (not intrinsic). This phenomenon is typical for sol−gel and base-catalyzed colloidal ZnO.[15,60]

Finally, through impedance spectroscopy, we compared the electrical properties of the deposited layers within a diode configuration consisting of ITO/ZnO/Spiro-OMeTAD/Ag (Figure S8 and Table S6). Both sputtered and CBD-grown ZnO films with comparable thicknesses show excellent blocking properties, with parallel resistance values extracted from the equivalent RC elements of $\sim 10^6$ Ω. Importantly, these values are ∼3 orders of magnitude higher than those measured for sol−gel and NPs-based ZnO,[61] which is in perfect agreement with the stronger n-type character of these latter films, as confirmed by UPS analysis.

The above characterizations highlight unambiguously that optical, structural, and electronic mimicry of sputtered ZnO was achieved under our optimized CBD conditions. To assess whether this deposition process is genuinely suitable for optoelectronic applications, we evaluated the two ZnO films as buffer layers within nanocrystal based CZTSSe solar cells prepared in a substrate configuration (see Figure 1).[44] The cross-sectional structure of such a device with our CBD grown ZnO is presented in Figure 5a,b. The CZTSSe layer is seen to

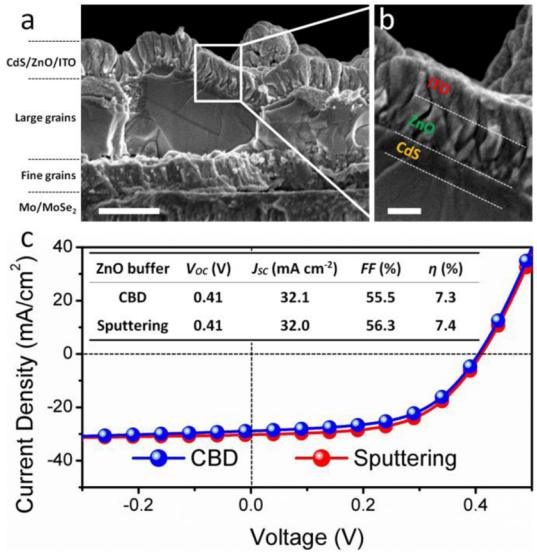

Figure 5. (a, b) Cross-sectional SEM images at different magnifications of a CZTSSe solar cell incorporating a ZnO buffer layer from CBD. The scale bars are 500 nm for image (a) and 100 nm for image (b). (c) *J*−*V* curves for a CZTSSe solar cell incorporating our solution-processed ZnO buffer layer and a reference cell prepared using a standard sputtered ZnO layer. The device parameters for the two cells are also reported.

be composed of a "large grain" microcrystalline top layer and a "fine grain" nanocrystalline underlayer. This microstructure is consistent with that reported extensively for CZTSSe films deposited from either NP inks or molecular precursors.[62−65] Figure 5b shows the columnar ZnO film conformal to the underlying p−n junction and covered with the ITO top contact. These SEM images confirm that even when using highly rough samples with nonplanar surfaces (typical of large

CZTSSe grains), high-quality buffer layers may be deposited using CBD. Figure 5c shows the current−voltage (J−V) characteristics of the completed solar cells. The device parameters demonstrate clearly that the open-circuit voltages (V_{OC}, ∼0.41 V), short circuit currents (J_{SC}, ∼32 mA cm^{-2}), fill factors (FF, ∼55%), and power conversion efficiencies (PCE, >7%) are nearly identical for both ZnO depositions.

CONCLUSION

In conclusion, we have presented a detailed investigation of the growth of ZnO thin films using a low-temperature chemical bath deposition method. Through careful manipulation of the thermodynamic and kinetic parameters of the chemical bath system, the microstructure and the properties of solution-processed ZnO were tuned to mimic those of ZnO produced via sputter coating. The mild, aqueous conditions used for the deposition, and the dense and highly oriented thin films that can be produced in this manner, provide clear processing advantages over existing vacuum-based depositions and a lucrative avenue for developing functional thin films. We have explicitly demonstrated this factor for high-efficiency, earth-abundant CZTSSe solar cells. This work serves to highlight the opportunity that exists of adopting solution processing within applications that currently rely on vacuum-based techniques, particularly where thin and conformal coatings are required.

ASSOCIATED CONTENT

Supporting Information

Additional characterizations and data: SEM, FTIR, XRD, UPS, ellipsometry, impedance spectroscopy, and profilometry. This material is available free of charge via the Internet at http://pubs.acs.org.

AUTHOR INFORMATION

Corresponding Authors

*E-mail: enrico.dellagaspera@csiro.au. (E.D.G.)
*E-mail: jacek.jasieniak@csiro.au. (J.J.J.)

Author Contributions

The manuscript was written through contributions of all authors. All authors have given approval to the final version of the manuscript.

Funding

This work was funded through the Manufacturing Flagship as part of Office of the Chief Executive Postdoctoral Fellowships (E.D.G. and J.v.E.). J.J.J. and A.S.R.C. acknowledge the Australian Research Council for funding through Grant No. DP110105341 and a Discovery Early Career Research Award, respectively. This work has been also partly f unded by the Australian Government through the Australian Renewable Energy Agency (ARENA).

Notes

The authors declare no competing financial interest.

ACKNOWLEDGMENTS

Part of this work was performed at the Melbourne Centre for Nanofabrication (MCN) in the Victorian Node of the Australian National Fabrication Facility (ANFF).

REFERENCES

(1) Sellinger, A.; Weiss, P. M.; Nguyen, A.; Lu, Y.; Assink, R. A.; Gong, W.; Brinker, C. J. Continuous Self-Assembly of Organic−Inorganic Nanocomposite Coatings that Mimic Nacre. *Nature* **1998**, *394*, 256−260.
(2) Caruso, R. A.; Antonietti, M. Sol-Gel Nanocoating:An Approach to the Preparation of Structured Materials. *Chem. Mater.* **2001**, *13*, 3272−3282.
(3) Pileni, M. P. The Role of Soft Colloidal Templates in Controlling the Size and Shape of Inorganic Nanocrystals. *Nat. Mater.* **2003**, *2*, 145−150.
(4) Cushing, B. L.; Kolesnichenko, V. L.; O'Connor, C. J. Recent Advances in the Liquid-Phase Syntheses of Inorganic Nanoparticles. *Chem. Rev.* **2004**, *104*, 3893−3946.
(5) Yin, Y.; Alivisatos, A. P. Colloidal Nanocrystal Synthesis and the Organic-Inorganic Interface. *Nature* **2005**, *437*, 664−670.
(6) Cozzoli, P. D.; Pellegrino, T.; Manna, L. Synthesis, Properties and Perspectives of Hybrid Nanocrystal Structures. *Chem. Soc. Rev.* **2006**, *35*, 1195−1208.
(7) Sanchez, C.; Boissière, C.; Grosso, D.; Laberty, C.; Nicole, L. Design, Synthesis, and Properties of Inorganic and Hybrid Thin Films Having Periodically Organized Nanoporosity. *Chem. Mater.* **2008**, *20*, 682−737.
(8) Søndergaard, R. R.; Hosel, M.; Krebs, F. C. Roll-to-Roll Fabrication of Large Area Functional Organic Materials. *J. Polym. Sci., Part B: Polym. Phys.* **2013**, *51*, 16−34.
(9) Kronenberg, N. M.; Steinmann, V.; Bürckstümmer, H.; Hwang, J.; Hertel, D.; Würthner, F.; Meerholz, K. Direct Comparison of Highly Efficient Solution- and Vacuum-Processed Organic Solar Cells Based on Merocyanine Dyes. *Adv. Mater.* **2010**, *22*, 4193−4197.
(10) Park, J. S.; Maeng, W.-J.; Kim, H.-S.; Park, J.-S. Review of Recent Developments in Amorphous Oxide Semiconductor Thin-Film Transistor Devices. *Thin Solid Films* **2012**, *520*, 1679−1693.
(11) Meyer, J.; Hamwi, S.; Kröger, M.; Kowalsky, W.; Riedl, T.; Kahn, A. Transition Metal Oxides for Organic Electronics: Energetics, Device Physics and Applications. *Adv. Mater.* **2012**, *24*, 5408−5427.
(12) Özgür, Ü.; Alivov, Ya. I.; Liu, C.; Teke, A.; Reshchikov, M. A.; Doğan, S.; Avrutin, V.; Cho, S.-J.; Morkoç, H. A Comprehensive Review of ZnO Materials and Devices. *J. Appl. Phys.* **2005**, *98*, 041301−103.
(13) Jagadish, C.; Pearton, S. *Zinc Oxide Bulk, Thin Films and Nanostructures − Processing Properties and Applications;* Elsevier: London, U.K., 2006.
(14) Klingshirn, C. ZnO: Material, Physics and Applications. *ChemPhysChem* **2007**, *8*, 782−803.
(15) Mashford, B. S.; Nguyen, T.-L.; Wilson, G. J.; Mulvaney, P. All-Inorganic Quantum-Dot Light-Emitting Devices Formed Via Low-Cost, Wet-Chemical Processing. *J. Mater. Chem.* **2010**, *20*, 167−172.
(16) Song, K.; Kim, D.; Li, X.-S.; Jun, T.; Jeong, Y.; Moon, J. Solution Processed Invisible All-Oxide Thin Film Transistors. *J. Mater. Chem.* **2009**, *19*, 8881−8886.
(17) Morfa, A. J.; Beane, G.; Mashford, B.; Singh, B.; Della Gaspera, E.; Martucci, A.; Mulvaney, P. Fabrication of ZnO Thin Films from Nanocrystal Inks. *J. Phys. Chem. C* **2010**, *114*, 19815−19821.
(18) Sun, Y.; Seo, J. H.; Takacs, C. J.; Seifter, J.; Heeger, A. J. Inverted Polymer Solar Cells Integrated with a Low-Temperature-Annealed Sol-Gel-Derived ZnO Film as an Electron Transport Layer. *Adv. Mater.* **2011**, *23*, 1679−1683.
(19) Jasieniak, J. J.; MacDonald, B. I.; Watkins, S. E.; Mulvaney, P. Solution-Processed Sintered Nanocrystal Solar Cells via Layer-by-Layer Assembly. *Nano Lett.* **2011**, *11*, 2856−2864.
(20) Della Gaspera, E.; Guglielmi, M.; Perotto, G.; Agnoli, S.; Granozzi, G.; Post, M. L.; Martucci, A. CO Optical Sensing Properties of Nanocrystalline ZnO−Au Films: Effect of Doping with Transition Metal Ions. *Sens. Actuators, B* **2012**, *161*, 675−683.
(21) Della Gaspera, E.; Guglielmi, M.; Martucci, A.; Giancaterini, L.; Cantalini, C. Enhanced Optical and Electrical Gas Sensing Response of Sol−Gel Based NiO−Au and ZnO−Au Nanostructured Thin Films. *Sens. Actuators, B* **2012**, *164*, 54−63.
(22) Lee, J.-H.; Park, B.-O. Transparent Conducting ZnO: Al, In and Sn Thin Films Deposited by the Sol−Gel Method. *Thin Solid Films* **2003**, *426*, 94−99.

(23) Ghosh, T.; Basak, D. Highly Efficient Ultraviolet Photodetection in Nanocolumnar RF Sputtered ZnO Films: a Comparison Between Sputtered, Sol-Gel and Aqueous Chemically Grown Nanostructures. *Nanotechnology* **2010**, *21*, 375202.
(24) Vayssieres, L.; Keis, K.; Lindquist, S.-E.; Hagfeldt, A. Purpose-Built Anisotropic Metal Oxide Material: 3D Highly Oriented Microrod Array of ZnO. *J. Phys. Chem. B* **2001**, *105*, 3350−3352.
(25) Govender, K.; Boyle, D. S.; Kenway, P. B.; O'Brien, P. Understanding the Factors that Govern the Deposition and Morphology of Thin Films of ZnO from Aqueous Solution. *J. Mater. Chem.* **2004**, *14*, 2575−2591.
(26) Schmidt-Mende, L.; MacManus-Driscoll, J. L. ZnO − Nanostructures, Defects, and Devices. *Mater. Today* **2007**, *10*, 40−48.
(27) Law, M.; Greene, L. E.; Johnson, J. C.; Saykally, R.; Yang, P. Nanowire Dye-Sensitized Solar Cells. *Nat. Mater.* **2005**, *4*, 455−459.
(28) Tsai, D.-S.; Lin, C.-A.; Lien, W.-C.; Chang, H.-C.; Wang, Y.-L.; He, J.-H. Ultra-High-Responsivity Broadband Detection of Si Metal-Semiconductor-Metal Schottky Photodetectors Improved by ZnO Nanorod Arrays. *ACS Nano* **2011**, *5*, 7748−7753.
(29) Boppella, R.; Anjaneyulu, K.; Basak, P.; Manorama, S. V. Facile Synthesis of Face Oriented ZnO Crystals: Tunable Polar Facets and Shape Induced Enhanced Photocatalytic Performance. *J. Phys. Chem. C* **2013**, *117*, 4597−4605.
(30) Kao, S.-H.; Tseng, Z.-L.; Ho, P.-Y.; Kao, C.-Y.; Thiyagu, S.; Lin, C.-F. Significance of the ZnO Nanorod Array Morphology for Low-Bandgap Polymer Solar Cells in Inverted Structures. *J. Mater. Chem. A* **2013**, *1*, 14641−14648.
(31) Jean, J.; Chang, S.; Brown, P. R.; Cheng, J. J.; Rekemeyer, P. H.; Bawendi, M. G.; Gradecak, S.; Bulovic, V. ZnO Nanowire Arrays for Enhanced Photocurrent in PbS Quantum Dot Solar Cells. *Adv. Mater.* **2013**, *25*, 2790−2796.
(32) Kim, K. S.; Jeong, H.; Jeong, M. S.; Jung, G. Y. Polymer-Templated Hydrothermal Growth of Vertically Aligned Single-Crystal ZnO Nanorods and Morphological Transformations Using Structural Polarity. *Adv. Funct. Mater.* **2010**, *20*, 3055−3063.
(33) Wang, M.; Kim, E. J.; Hahn, S. H.; Park, C.; Koo, K.-K. Controlled Crystal Growth and Crystallite Orientation in ZnO Films/Nanorods Prepared by Chemical Bath Deposition: Effect of Solvent. *Cryst. Growth Des.* **2008**, *8*, 501−506.
(34) Klenk, R. Characterisation and Modelling of Chalcopyrite Solar Cells. *Thin Solid Films* **2001**, *387*, 135−140.
(35) Jahagirdar, A. H.; Kadam, A. A.; Dhere, N. G. In *Role of i-ZnO in Optimizing Open Circuit Voltage of CIGS2 and CIGS Thin Film Solar Cells.* Photovoltaic Energy Conversion, Conference Record of the 2006 IEEE 4th World Conference; IEEE: New York, **2006**, *1*, 557−559.
(36) Winkler, M. T.; Wang, W.; Gunawan, O.; Hovel, H. J.; Todorov, T.; Mitzi, D. Optical Designs That Improve the Efficiency of $Cu_2ZnSn(S,Se)_4$ Solar Cells. *Energy Environ. Sci.* **2014**, *7*, 1029−1036.
(37) Rau, U.; Schmidt, M. Electronic Properties of ZnO/CdS/Cu(In,Ga)Se2 Solar Cells - Aspects of Heterojunction Formation. *Thin Solid Films* **2001**, *387*, 141−146.
(38) Scheer, R.; Messmann-Vera, L.; Klenk, R.; Schock, H.-W. On the Role of Non-Doped ZnO in CIGSe Solar Cells. *Prog. Photovoltaics* **2012**, *20*, 619−624.
(39) Ki, W.; Hillhouse, H. W. Earth-Abundant Element Photovoltaics Directly from Soluble Precursors with High Yield Using a Non-Toxic Solvent. *Adv. Energy Mater.* **2011**, *1*, 732−735.
(40) Wang, G.; Wang, S.; Cui, Y.; Pan, D. A Novel and Versatile Strategy to Prepare Metal−Organic Molecular Precursor Solutions and Its Application in $Cu(In,Ga)(S,Se)_2$ Solar Cells. *Chem. Mater.* **2012**, *24*, 3993−3997.
(41) Akhavan, V. A.; Goodfellow, B. W.; Panthani, M. G.; Steinhagen, C.; Harvey, T. B.; Stolle, C. J.; Korgel, B. A. Colloidal CIGS and CZTS Nanocrystals: A Precursor Route to Printed Photovoltaics. *J. Solid State Chem.* **2012**, *189*, 2−12.
(42) Todorov, T. K.; Tang, J.; Bag, S.; Gunawan, O.; Gokmen, T.; Zhu, Y.; Mitzi, D. B. Beyond 11% Efficiency: Characteristics of State-of-the-Art $Cu_2ZnSn(S,Se)_4$ Solar Cells. *Adv. Energy Mater.* **2013**, *3*, 34−38.
(43) Schnabel, T.; Löw, M.; Ahlswede, E. Vacuum-Free Preparation of 7.5% Efficient $Cu_2ZnSn(S,Se)_4$ Solar Cells Based on Metal Salt Precursors. *Sol. Energy Mater. Sol. Cells* **2013**, *117*, 324−328.
(44) van Embden, J.; Chesman, A. S. R.; Della Gaspera, E.; Duffy, N. W.; Watkins, S. E.; Jasieniak, J. J. $Cu_2ZnSnS_{4x}Se_{4(1-x)}$ Solar Cells from Polar Nanocrystal Inks. *J. Am. Chem. Soc.* **2014**, *136*, 5237−5240.
(45) Liu, D.; Kelly, T. L. Perovskite Solar Cells with a Planar Heterojunction Structure Prepared Using Room-Temperature Solution Processing Techniques. *Nat. Photonics* **2014**, *8*, 133−138.
(46) Wood, A.; Giersig, M.; Hilgendorff, M.; Vilas-Campos, A.; Liz-Marzan, L. M.; Mulvaney, P. Size Effects in ZnO: The Cluster to Quantum Dot Transition. *Aust. J. Chem.* **2003**, *56*, 1051−1057.
(47) Greene, L. E.; Law, M.; Tan, D. H.; Montano, M.; Goldberger, J.; Somorjai, G.; Yang, P. General Route to Vertical ZnO Nanowire Arrays Using Textured ZnO Seeds. *Nano Lett.* **2005**, *5*, 1231−1236.
(48) Tian, Z. R.; Voigt, J. A.; Liu, J.; Mckenzie, B.; Mcdermott, M. J.; Rodriguez, M. A.; Xu, H. Complex and Oriented ZnO Nanostructures. *Nat. Mater.* **2003**, *2*, 821−826.
(49) Joo, J.; Chow, B. Y.; Prakash, M.; Boyden, E. S.; Jacobson, J. M. Face-selective Electrostatic Control of Hydrothermal Zinc Oxide Nanowire Synthesis. *Nat. Mater.* **2011**, *10*, 596−601.
(50) Woll, C. The Chemistry and Physics of Zinc Oxide Surfaces. *Prog. Surf. Sci.* **2007**, *82*, 55−120.
(51) Akhter, S.; Lui, K.; Kung, H. H. Comparison of the Chemical Properties of the Zinc-Polar, the Oxygen-Polar, and the Nonpolar Surfaces of ZnO. *J. Phys. Chem.* **1985**, *89*, 1958−1964.
(52) Cao, B.; Cai, W. From ZnO Nanorods to Nanoplates: Chemical Bath Deposition Growth and Surface-Related Emissions. *J. Phys. Chem. C* **2008**, *112*, 680−685.
(53) McPeak, K. M.; Le, T. P.; Britton, N. G.; Nickolov, Z. S.; Elabd, Y. A.; Baxter, J. B. Chemical Bath Deposition of ZnO Nanowires at Near-Neutral pH Conditions without Hexamethylenetetramine (HMTA): Understanding the Role of HMTA in ZnO Nanowire Growth. *Langmuir* **2011**, *27*, 3672−3677.
(54) Lincot, D. Solution Growth of Functional Zinc Oxide Films and Nanostructures. *MRS Bull.* **2010**, *35*, 778−789.
(55) Yan, X.; Li, Z.; Chen, R.; Gao, W. Template Growth of ZnO Nanorods and Microrods with Controllable Densities. *Cryst. Growth Des.* **2008**, *7*, 2406−2410.
(56) Barret, C.; Massalski, T. B. *Structure of Metals;* Pergamon Press: Oxford, U.K., 1980, 1923.
(57) Lide, D. R. *CRC Handbook of Chemistry and Physics,* 87th ed; Taylor and Francis: Boca Raton, FL, 2007, 10−248.
(58) Bruggeman, D. A. G. Berechnung Verschiedener Physikalischer Konstanten von Heterogenen Substanzen. *Ann. Phys. (Leipzig, Ger.)* **1935**, *24*, 636−679.
(59) Nyquist, R. A.; Kagel, R. O. *Handbook of Infrared and Raman Spectra of Inorganic Compounds and Organic Salts;* Academic Press: San Diego, CA, 1997.
(60) Bong, H.; Lee, W. H.; Lee, D. Y.; Kim, B. J.; Cho, J. H.; Cho, K. High-Mobility Low-Temperature ZnO Transistors with Low-Voltage Operation. *Appl. Phys. Lett.* **2010**, *96*, 192115.
(61) Morfa, A. J.; MacDonald, B. I.; Subbiah, J.; Jasieniak, J. J. Understanding the Chemical Origin of Improved Thin-Film Device Performance from Photodoped ZnO Nanoparticles. *Sol. Energy Mater. Sol. Cells* **2014**, *124*, 211−216.
(62) Guo, Q.; Ford, G. M.; Yang, W. C.; Walker, B. C.; Stach, E. A.; Hillhouse, H. W.; Agrawal, R. Fabrication of 7.2% Efficient CZTSSe Solar Cells Using CZTS Nanocrystals. *J. Am. Chem. Soc.* **2010**, *132*, 17384−17386.
(63) Cao, Y.; Denny, M. S., Jr.; Caspar, J. V.; Farneth, W. E.; Guo, Q.; Ionkin, A. S.; Johnson, L. K.; Lu, M.; Malajovich, I.; Radu, D.; Rosenfeld, H. D.; Choudhury, K. R.; Wu, W. High-Efficiency Solution-Processed $Cu_2ZnSn(S,Se)_4$ Thin-Film Solar Cells Prepared from Binary and Ternary Nanoparticles. *J. Am. Chem. Soc.* **2012**, *134*, 15644−15647.
(64) Zhou, H.; Song, T.-B.; Hsu, W.-C.; Luo, S.; Ye, S.; Duan, H.-S.; Hsu, C.-J.; Yang, W.; Yang, Y. Rational Defect Passivation of $Cu_2ZnSn(S,Se)_4$ Photovoltaics with Solution-Processed

Cu_2ZnSnS_4:Na Nanocrystals. *J. Am. Chem. Soc.* **2013**, *135*, 15998−16001.
(65) Romanyuk, Y. E.; Fella, C. M.; Uhl, A. R.; Werner, M.; Tiwari, A. N.; Schnabel, T.; Ahlswede, E. Recent Trends in Direct Solution Coating of Kesterite Absorber Layers in Solar Cells. *Sol. Energy Mater. Sol. Cells* **2013**, *119*, 181−189.